An Adaptive Multi-Scale Retinex Algorithm Realizing High Color Quality and High-Speed Processing

Tatsumi Watanabe*, Yasuhiro Kuwahara, Akio Kojima, and Toshiharu Kurosawa▲
AV Core Technology Development Center, Matsushita Electric Industrial Co., Ltd., Osaka, JAPAN

With the popularity of digital still cameras (DSCs), improvement of image quality in dark areas of the image is needed. There are two typical techniques for this: gamma correction and histogram equalization. However, such techniques are not always sufficient to improve scene detail in dark areas. Recently, examinations of Retinex theory taking into account the human vision model proposed by Land are being given attention. This algorithm, which utilizes spatial information between surrounding pixels, gives good image detail. Single-scale Retinex (SSR) and Multi-scale Retinex (MSR) are typical Retinex algorithms. However, they raise several practical use issues concerning color images reproduced by printers. In order to address such issues, Adaptive Multi-scale Retinex (AMSR) synthesis of images originally processed by MSR to the original image has been proposed. This algorithm consists of two processes, linear computation and synthesis of both the original image and the image processed by MSR. AMSR can be compared to histogram equalization and MSR for DSC images. AMSR shows that visibility in dark areas can be improved compared to other techniques. Moreover, NEW-AMSR has the following two features: suppression of chromatic unbalance in R, G and B channels, and a high speed processing technique to compute a weighted average.

Journal of Imaging Science and Technology 49: 486–497 (2005)

Introduction

It has recently been suggested that the image quality of digital still cameras (DSCs) is close to the good image quality of a silver halide photograph. However, the issue of a narrow dynamic range has been pointed out with respect to DSC images. This means that DSC images are poor in scene detail and color reproduction in dark areas. Especially in the case of a scene that contains both bright and dark areas, it is hard to obtain a beautiful image, and some type of correction technique is required.

Typical correction techniques such as gain/offset correction[1,2] and histogram equalization[3,4] have already been utilized for such images. Gain/offset correction is linear processing to attain a wide dynamic range for DSC images. This technique linearly creates a wide dynamic range for images so as to expand the maximum luminance range of the display medium. However, it does not always provide good visual perception for the original scene. Histogram equalization is based on the idea of transforming an input image to an output image that contains a uniform luminance distribution. This technique works well for images with unimodal or weak bimodal histograms, but does not work so well for images with strong bimodal histograms, i.e., images containing both very bright and very dark regions.

Another well known technique used for providing dynamic range compression is the application of nonlinear transforms such as gamma nonlinearity, a logarithmic function, and a power law function to the input image.[1,2] These functions are typically biased toward increasing visibility in dark areas by sacrificing visibility in bright areas. However, the selection of nonlinear transforms is dependent on the luminance distribution in the input image, and the luminance in bright areas tends to be saturated.

The following technique has also been proposed. Bright and dark scenes are taken separately by a different shutter speed and iris diaphragm in a DSC. The middle tone is generated by the synthesis of these images and a wide dynamic range is realized. This technique generates blur and distortion in the output image due to the time required to take at least two images in sequence; it is impossible in principal to take the same image twice.

The above-mentioned techniques are not always effective for tone mapping because they utilize pixel-to-pixel processing without consideration of the surrounding scenes in an image. This means that it is necessary to utilize spatial information in the image in order to reproduce a visually natural and a good contrast image as seen by human eyes.[5]

Recently, theories which take human eye characteristics into consideration are being given attention, including the so-called Retinex theory that was proposed by Land. It has been extended to space-to-pixel conversion theory which takes into account the surrounding pixels of a pixel under consideration.[6,7]

Original manuscript received July 12, 2004

IS&T Member

Corresponding author: T. Watanabe, Watanabe.tatsumi@panasonic.com

Hurlbert[8] studied the properties of Land's first Retinex model and other lightness theories and found that they share a common mathematical foundation but cannot actually compute reflectance for arbitrary scenes. Moore et al.[9] took up Retinex as a natural implementation for analog very large-scale integration (VLSI) resistive networks and found that color rendition was dependent on scene content – whereas some scenes worked well, others did not. These studies also pointed out the problems that occur due to color Mach bands and the graying-out of large uniform areas of color.

McCann[10] proposed a technique based on Retinex theory; Funt et al.[11] provided Matlab code for McCann's Retinex. These techniques create a multi-resolution pyramid from the input by averaging image data. It begins the pixel comparisons at the most highly averaged, or top level of the pyramid. After computing luminance on the image at a reduced resolution, the resulting luminance values are propagated down, by pixel replication, to the pyramid's next level as initial luminance estimates at that level. Further pixel comparisons refine the luminance estimates at the higher resolution level and then those new luminance estimates are again propagated down a level in the pyramid. This process continues until values have been computed for the pyramid's bottom level. To acquire an output image with high quality, this technique needs a suitable output lookup table function and a number of iterations at each level of multi-level computation.

Moreover, Jobson and others have evolved Land's theory to Single-scale Retinex (SSR) and Multi-scale Retinex (MSR).[12–17] MSR is a technique combined with several output images processed by SSR in order to satisfy good dynamic range compression and good tonal rendition. However, there are some issues in terms of color correction of images having a different intensity distribution for the RGB channel. In particular, the following issues are involved in practical use: a) setting many parameters, b) a decrease of luminance caused by slight luminance deviation in a bright area, c) chromatic unbalance in R, G and B channels, d) instability of the logarithmic computation in MSR, and e) a blurred edge and noise appearance in a dark area.[18]

In order to address these issues, Adaptive Multi-scale Retinex (AMSR) for synthesizing the image processed by MSR to the original image has been studied, and an automatic contrast adjustment technique in accordance with the input image has been developed.

In this article, experimental results regarding the highly accurate color balance and high speed processing of a new technique named NEW-AMSR are described in comparison with conventional techniques, and the effectiveness of AMSR is shown from the results visually evaluated on the output images of each technique.

Overview of Retinex Theory

This section provides an overview of the SSR technique based on Retinex theory as proposed by Jobson et al. The technique is extended from SSR to MSR[12–17] with multiple kernel windows (scales) of different sizes.

Retinex Theory

Retinex theory[6,7] is the basis of SSR and MSR. The basic principle is shown schematically in Fig. 1. The diagram presents an explanation of the reflectance change for a gray-step image, but it is possible to extend it to color images. In Figs. 1(a), 1(b), and 1(c) we show the reflectance intensity of the gray-step image, the intensity of inverse continuous illumination in accordance with the gray-step image, and the resultant reflectance intensity superimposed on both the reflectance intensities of Figs. 1(a) and 1(b), respectively. The signal of the superimposed reflectance intensity is not the same as the intensity shown in Fig. 1(a), but the appearance to human vision is the same as that of the gray-step image. It is a fact that even if the reflectance intensity is the same signal, a small difference in reflectance intensity between adjacent gray images is perceived as a relative ratio of the adjacent reflectance for human vision. Moreover, the relative difference of lightness and darkness between two spatially separated pixels could be computed as the chain of the relative ratio between the adjacent reflectance according to the course. This model was extended to a technique computing the relative ratio of reflectance between the gazing point (Center) and the surrounding pixels (Surround), and it is called the Center/Surround or C–S technique.

Single-Scale Retinex

Single-scale Retinex (SSR) was the technique proposed by Jobson et al., and it was the technique used for extension to the C–S technique. Figure 2 shows a diagram of SSR. The Retinex output $SR_i(x,y)$ of SSR is given by

$$SR_i(x,y) = \log I_i(x,y) - \log\{F(x,y) * I_i(x.y)\} \tag{1}$$

$$F(x,y) = Ke^{-(x^2+y^2)/c^2} \tag{2}$$

$$\iint F(x,y)dxdy = 1 \tag{3}$$

where $I_i(x, y)$ is the image distribution in the i-th spectral band for each coordinate position (x, y); symbol "*" denotes the convolution operation. $F(x, y)$ is the surrounding function applying to each coordinate position (x, y) and given by Eq. (2). The coefficient c in Eq. (2) represents the standard deviation for the surrounding field or the scale. K is the normalized constant coefficient determined so as to satisfy the condition in Eq. (3).

From Eqs. (1) and (3), the second term in Eq. (1) is equivalent to a weighted average value of the intensity of the surrounding pixels for a pixel under consideration. $F(x, y)$ is given by a Gaussian function in order to take into account global contributions at each position of the pixels. In addition, the surrounding function $F(x, y)$ enhances the characteristics of the regional contributions.

Multi-Scale Retinex

SSR is strongly influenced by the surrounding function $F(x,y)$ with the scale value c, so it is necessary to consider a suitable scale value c in accordance with the dynamic range of the pixel value in input images.

Multi-scale Retinex (MSR) was also proposed by Jobson et al. as an advanced SSR. The Retinex output $MR_i(x,y)$ of MSR is given by Eq. (4), (5), and (6).

$$MR_i(x,y) = \sum_{s=0}^{nn-1} w_s \cdot (\log I_i(x,y) - \log\{F_s(x,y) * I_i(x,y)\}) \tag{4}$$

$$F_s(x,y) = K_s e^{-(x^2+y^2)/c_s^2} \tag{5}$$

$$\iint F_s(x,y)dxdy = 1 \tag{6}$$

where nn is the number of scales, w_s is the weight coefficient associated with the output by SSR with the scale

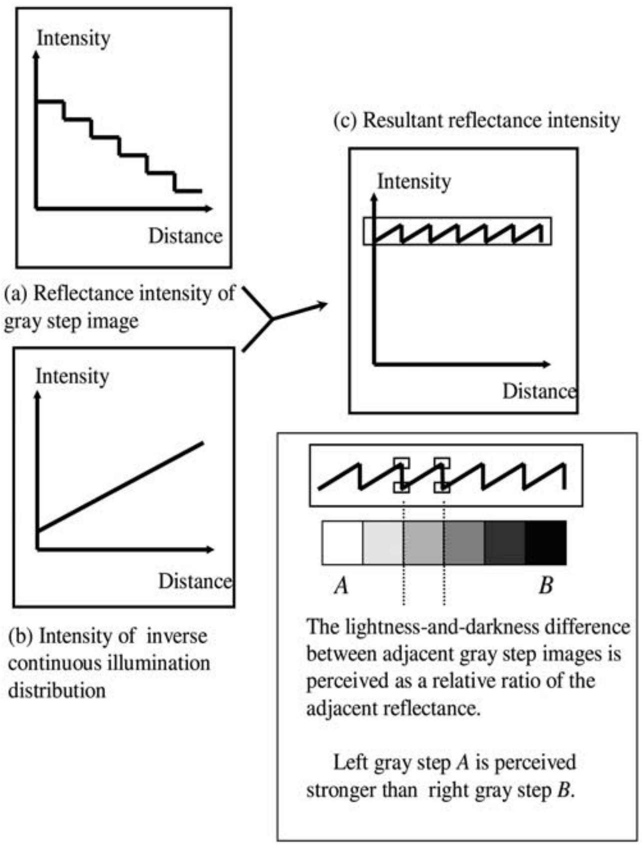

Figure 1. Diagram of Retinex Theory

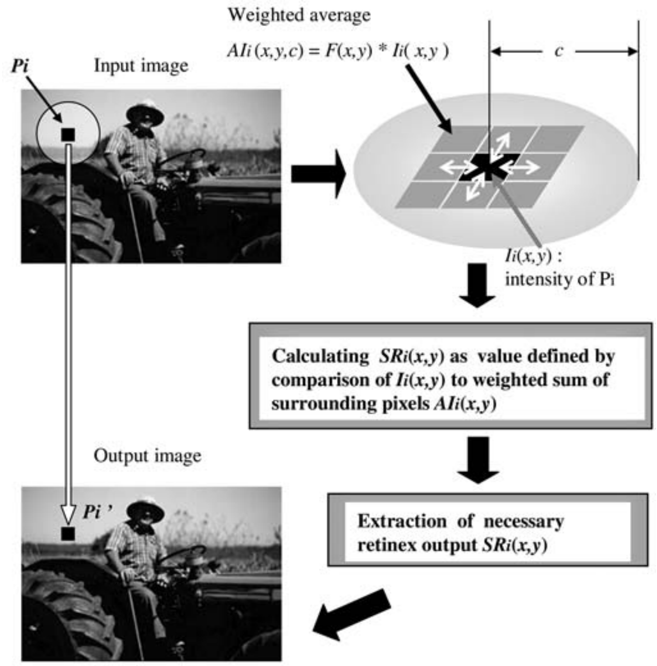

Figure 2. Diagram of SSR Technique

c_s. The Retinex output $MR_i(x, y)$ is calculated by the weighted sum of several SSR-outputs in the various scales. Since MSR can give an arbitrary amount of dynamic range compression, it offers stable contrast conversion without dependency of the scale value. The weight w_s is satisfied by $\sum_s w_s = 1$.

Figure 3 shows a diagram of SSR expanded to MSR. Furthermore, since a chromatic unbalance might be caused by Eq. (4), (5) and (6), Jobson proposed the technique using Retinex output $MR_i'(x, y)$ given by Eq. (7).

$$MR_i'(x,y) = MR_i \cdot \left(1 + C \cdot I_i(x,y) \Big/ \sum I_i(x,y)\right), \quad C = 125 \qquad (7)$$

However, MSR still includes the following concerns:[18]

- Proposed Retinex output $MR_i(x, y)$ includes the logarithmic computation as shown in Eq. (4). Therefore, the Retinex output level is unstable with respect to both noise in a dark area and the deviation for the offset level of the input devices being a zero signal.
- Chromatic unbalance in R, G and B channels occurs in output images.
- Since clipping of the highest and lowest signal in the histogram signal of Retinex output is applied in Eq. (7), the selection of the clipping points becomes important. First, the upper and lower levels of the Retinex output $MR_i(x, y)$ are clipped, then the gain/offset correction is carried out to the clipped Retinex output. This means that it is hard to set gain/offset levels and also hard to control suitable gain/offset parameters for a number of input images.

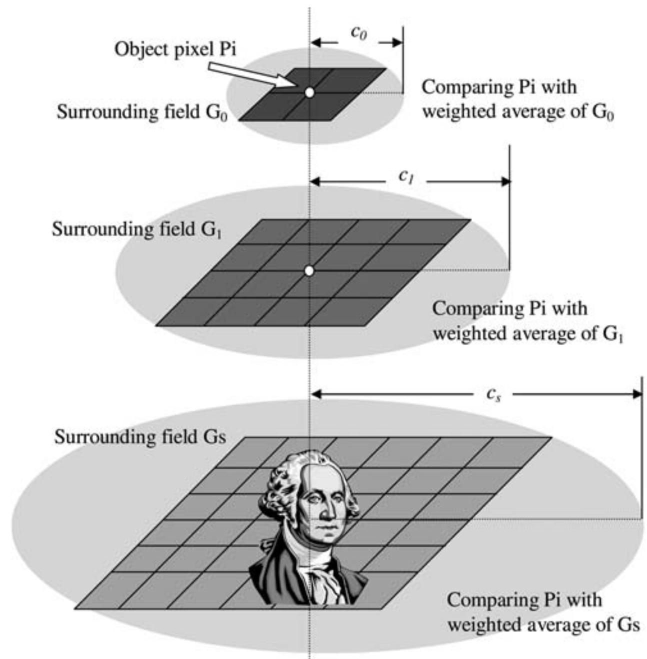

Figure 3. Diagram Expanded into MSR Technique

- In case intensity change is small over a wide area, a drop in luminance occurs over the wide area of the output image.
- Color noise in dark areas tends to be emphasized.

As indicated above, Jobson's MSR output image quality is strongly influenced by the adjustment of many parameters. Therefore, suitable empirical parameters are needed.

Adaptive Multi-Scale Retinex (AMSR)

Adaptive Multi-scale Retinex (AMSR) solves the MSR issues described above. AMSR is an algorithm that synthesizes the image processed by MSR to the original image. The algorithm is presented by Eqs. (8), (9), (10) and (11). Figure 4 shows a schematic diagram of the AMSR technique process.

$$AR_i(x,y) = \sum_s w_s \, {I_i(x,y)} \big/ {Ak(x,y,c_s)} \tag{8}$$

$$Ak(x,y,c_s) = k(x,y) * F_s(x,y) \tag{9}$$

$$Deki(x,y) = \sum_s w_s \cdot eBaisu \cdot \left({I_i(x,y)} \big/ {Ak(x,y,c_s)} - 1.0 \right) \times Adk(x,y,c_s) \tag{10}$$

$$u(x,y) = u_{\max} \times \exp\left(- {k(x,y)^2} \big/ {TH^2} \right) \tag{11}$$

$$O_i(x,y) = (1 - u(x,y)) \times I_i(x,y) + u(x,y) \times E_i(x,y) \tag{12}$$

A. The maximum and minimum luminance values *THHigh* and *THLow* are set when the weighted average luminance $Ak(x,y,c_s)$ in the scale window c_s of the image is calculated and the luminance of a pixel in the surrounding field is set between *THHigh* and *THLow*. Using this process, an abrupt drop of Retinex output $ARi(x,y)$ in a bright area where luminance changes a little can be suppressed by setting the maximum luminance value. An abrupt rise of Retinex output $ARi(x, y)$ in a dark area with a little change can be suppressed by setting the minimum luminance value.

B. The Retinex output $ARi(x, y)$ is calculated by the ratio of each component for the weighted average luminance $Ak(x, y, c_s)$ in the scale window c_s of the image as shown in Eq. (8). $k(x,y)$ is the luminance for the pixel coordinate position (x, y). The surrounding function $Fs(x, y)$ in Eq. (9) is calculated by Eqs. (5) and (6). Eq. (8) is equivalent to two steps: 1) calculation of the ratio of each component for luminance, and 2) multiplication of the ratio of the luminance for the weighted average luminance $Ak(x, y, c_s)$ to the ratio of each component for the luminance. The chromatic unbalance in the output images is suppressed by this technique, and an unstable output image due to logarithmic conversion is also suppressed. MSR has two merits: compression for the Retinex output range and easy extraction to the middle tone. However, unstable states are easily caused by noise in the brightness level of the image. Therefore, in order to offset this influence, the linear computation model shown in Eq. (8) has been adopted.

C. The emphasis image in Fig. 4 is acquired by using $Ak(x, y, c_s)$. $Ei(x, y)$ in the emphasis image is the image distribution in the i-th spectral band for each coordinate position (x, y). $Ei(x, y)$ is calculated by multiplication of the transform value *Ct* to $ARi(x, y)$. $Ak(x, y, c_s)$ in the scale window c_s is calculated by Eq. (9). This processing is to reduce the effect of the device calibration to transform the Retinex output $ARi(x, y)$ to the intensity of the pixel. *Ct* is a constant value to transform $ARi(x, y)$ to the intensity of the pixel in the emphasized image. The value near the center value in the dynamic range of the intensity of the pixel is generally selected as *Ct*.

D. As shown in the process (E), the image emphasized by process (C) and the input image are synthesized. As a result of process (E), a blurred edge tends to occur. In order to retain fine edges, edge emphasized components are added to Retinex output $ARi(x, y)$. $Adk(x, y, c_s)$ is defined as the average value of the absolute luminance change in the surrounding pixels for the luminance of the pixel under consideration. Retinex output $ARi(x, y)$ in process (B) is corrected by using the edge emphasis component $Deki(x, y)$. A edge component of the i-th spectral band $Ii(x, y)$ is connected with to the relative value of $Ii(x, y)$ for the weighted average luminance $Ak(x, y, c_s)$ at each coordinate position (x, y). And when $Ii(x, y)$ is nearly equivalent to $Ak(x, y, c_s)$, the edge component of the i-th band become small. Therefore, $Deki(x, y)$ is calculated by Eq. (10) to emphasize this edge component. *eBaisu* in Eq. (10) is a positive constant between 0.0 and 1.0. An edge component of the i-th band is emphasized according to the average value of the absolute luminance change, so that the intensity of i-th spectral band $Ii(x, y)$ is larger than the weighted average luminance $Ak(x, y, c_s)$ for each coordinate position (x, y). On the contrary, an edge component of the i-th band is suppressed, so that the intensity of the i-th spectral band $Ii(x, y)$ is smaller than the weighted average luminance $Ak(x, y, c_s)$.

E. The image emphasized by process (C) and the original image are synthesized. Since an abrupt rise in luminance results from this synthesis, the weighted coefficient applied to the emphasis image is controlled by the input luminance value for the pixel under consideration. The synthesis coefficient $u(x, y)$ in the emphasized image is presumed by Eq. (11). The synthesis coefficient $u(x, y)$ has a value between 0.0 and 1.0. *TH* in Eq. (11) is a positive constant. $u_{\max}$ in Eq. (11) is the maximum value of $u(x, y)$, and $u_{\max}$ is controlled by the luminance value synthesized in this process. When the luminance in the input image is low, $u(x, y)$ is set to large value. On the contrary, when the luminance in input image is high, $u(x, y)$ is set to a small value. In Fig. 4, $Oi(x, y)$ and $Ei(x, y)$ show the image distribution in the i-th spectral band for each coordinate position (x, y) in the synthesized image and that in the emphasized image respectively. $Oi(x, y)$ is calculated by synthesizing $Ii(x, y)$ and $Ei(x, y)$ using Eq. (12). These equations show that the effect of an emphasis image is strengthened for the intensity of the pixel in the output image when the luminance in the input image is low. On the contrary, when the luminance in the input image is high, the effect of an emphasis image is weakened in the output image.

F. When comparing the input luminance value with the luminance value of the image synthesized by process (E), in case the luminance of the synthesized image is lower than the input luminance value, the luminance synthesized in process (E) is transposed to the input luminance, and it correspondingly changes in the R, G and B channels.

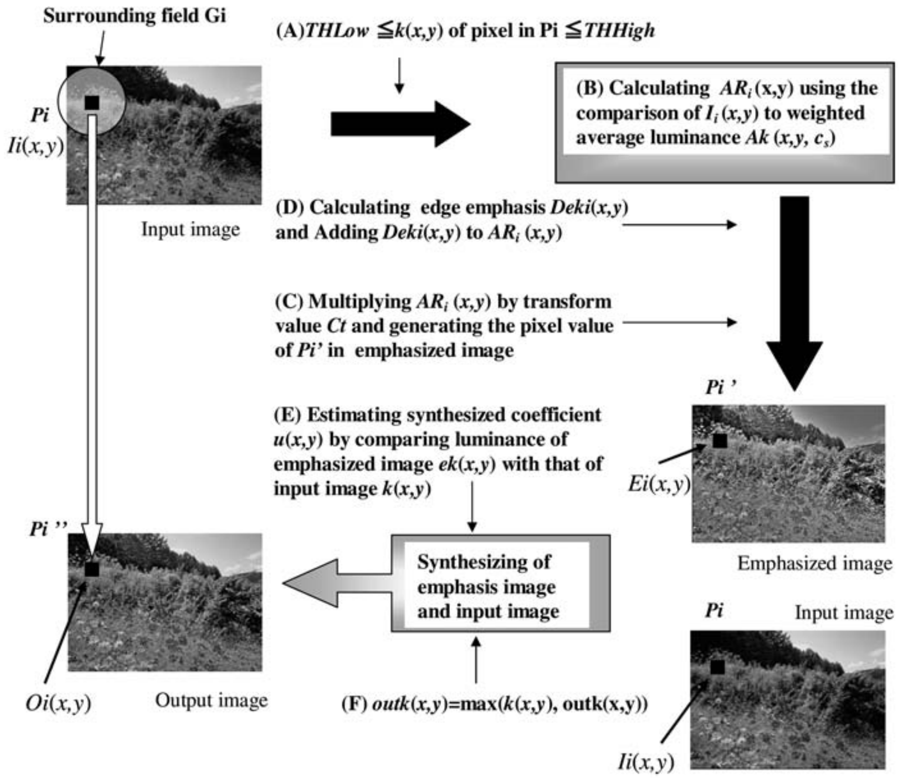

Figure 4. Schematic Diagram of AMSR Technique

Sample 1 Sample 2

Figure 5. Original Images for Simulation Experiments

Processes (A), (C) and (E) are intended to suppress both a drop in luminance in the area of the high uniform luminance level and color noise generated by an abrupt rise in the low uniform luminance level. Furthermore, color saturation generated in the near edge area in the emphasis image can also be suppressed by synthesizing both the input image and the emphasized image, as shown in process (E).

Simulation Results

Simulation Conditions and Experiments

Images taken with a commercial DSC, an Epson CP-920Z, were simulated. Figure 5 shows samples of the original images used for the simulations. The sample images are constructed with three spectral bands – red, green and blue. Each band is 8 bits. The sample images were reduced by Adobe Photoshop 6.0 software from an original size of 2048 × 1536 pixels to 450 × 338 pixels. Gain/offset correction, histogram equalization, MSR and AMSR were simulated and AMSR was evaluated compared to these techniques.

For AMSR and MSR, a scale number of nn = 3 was selected. The size of the scales was c_0 = 126, c_1 = 30 and c_2 = 6. C_t in AMSR shows the fundamental value transforming the Retinex output to the intensity of the pixel, and C_t = 128 was selected. *THHigh* was set to 200, and *THLow* was set to 20.

Evauations

We visually evaluated AMSR compared with the conventional techniques. Figure 6 shows the resultant images simulated by (a) gain/offset

Figure 6. Output Images Processed by (a) Gain/Offset Correction; (b) Histogram Equalization; (c) Jobson MSR Technique; and (d) AMSR Technique.

correction, (b) histogram equalization, (c) MSR, and (d) AMSR, respectively.

In the case of the night scene shown in Fig. 6, the image for (a) gain/offset correction shows almost no improvement. The image for (b) histogram equalization is much too bright in all areas. The dark area is clearly rendered in the image for MSR shown in (c), but color noise has appeared in the night scene image. Color noise cannot be avoided in principle because it is included in the signal of the DSC's CCD imaging sensors. In the original image (a) shown in Fig. 5, the color noise in the dark areas is not conspicuous since the background area is in the low luminance level. However, color noise is more conspicuous in the MSR image. Comparing the resultant images of (a), (b) and (c), the visibility of the image for (d) AMSR is clearly improved and it maintains good color balance that is similar to the atmosphere of the original image.

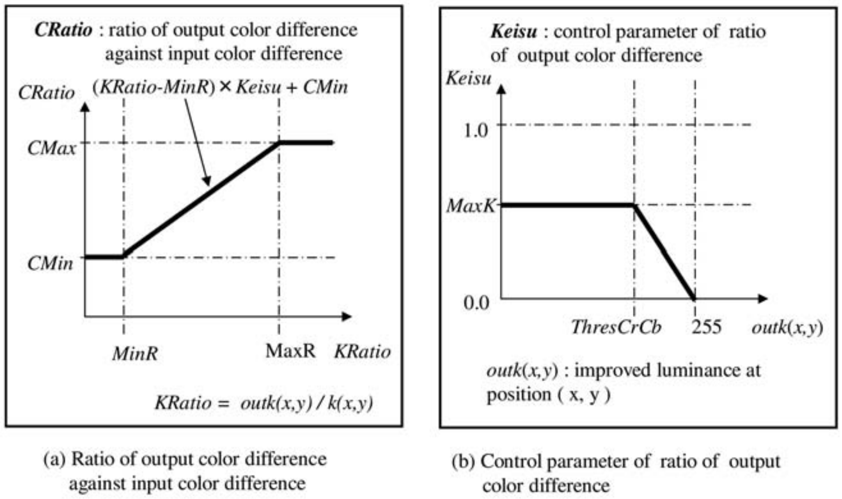

(a) Ratio of output color difference against input color difference

(b) Control parameter of ratio of output color difference

Figure 7. Diagram of Control Function for Color Difference

For the portrait images in Fig. 6, the same result as that of the night scene image was recognized visually. Compared to the original image in Fig. 5(b), the image for (a) gain/offset correction shows little improvement in terms of contrast. With (b) histogram equalization, there is a noticeable drop in luminance. In the image for (c) MSR, contrast detail is excessively enhanced, and visible “halo” artifacts, i.e., an overflow of intensity close to the boundary of trees and people, can be observed.

In the image for (d) AMSR, the contrast is adequately enhanced, and “halo” artifacts around the boundary of the people do not occur. The facial areas are also clearly reproduced. On the other hand, in the image for (c) MSR, there is a drop in luminance in the area with a high uniform luminance level. This occurs, for example, in the sky areas and the building wall areas. The AMSR image shows that a drop in luminance for the sky areas and the building walls has been suppressed.

From the above discussion, by visual evaluations we found that the overall image quality of AMSR shows an improvement over gain/offset correction, histogram equalization and MSR techniques. In addition, experiments have been conducted using many image samples and various surrounding scales. Similar results have been observed.

Improvement of Color Appearance and Processing Speed

In this section, we discuss improvement of color appearance and the processing speed of AMSR.

- In the case of considerable deviations between the individual R, G and B channels of an image, the deviations are emphasized more and the chromatic unbalance between each spectral band is not sufficiently suppressed.
- Both MSR and AMSR have a long processing time because of the large size of the surrounding filter.

Improvement of Color Appearance

In AMSR, the ratio of each RGB component in both the output image and the input image is equal. AMSR can thus maintain the ratio of components against luminance in the input image in comparison to conventional MSR.

However, when the RGB value in a dark area is abruptly emphasized, it is possible to see a cyan color in the dark area. Figure 9(b) provides an example of poor color appearance. This is particularly noticeable in the area within the red line. This effect could be caused by strong emphasis of the differences between the R, G and B channels of the image.

In general, the input image of a DSC is composed of pixel values in the R, G and B channels. However, from the human vision point of view, it may be said that in spite of the component values in the input image, the impression of color is influenced by color difference between each component. Therefore, pixel values R, G, and B in the input image are changed into luminance component $k(x, y)$ and two components of color difference Cr and Cb, which are closely related to human vision. Next, improved processing of the luminance $k(x, y)$ in a dark area is calculated according to the characteristics of human vision. This processing is obtained by applying AMSR to enhancement of the luminance component in the input image.

Then, the improvement ratio of the color difference $CRatio$ is controlled by the improvement ratio $KRatio$ between the output and input luminance. The control function for the improvement ratio of color difference is executed according to the diagram shown in Fig. 7. In Eq. (13), $CMax$ and $CMin$ show the maximum ratio of color difference and the minimum ratio of color difference, respectively. In addition, $outK(x, y)$ is the improvement luminance at position (x, y).

$$CRatio = \begin{cases} CMax & if\ KRatio \geq MaxR \\ CMin & if\ KRatio \leq MinR \\ (KRatio - MinR) \times Keisu + CMin & otherwise \end{cases} \quad (13)$$

As shown in Fig. 7(a), $CRatio$ is set between the minimum improvement ratio $CMinR$ and the maximum improvement ratio $CMaxR$, and it is linearly controlled against $KRatio$ between $MinR$ and $MaxR$. $MinR$ and $MaxR$ are positive constants.

$$Keisu(outkido) = \begin{cases} MaxK & if\ outK \leq ThresCrCb \\ MaxK - MaxK \times {(255 - ThresCrCb)}\big/{(outK - ThresCrCb)} & otherwise \end{cases} \quad (14)$$

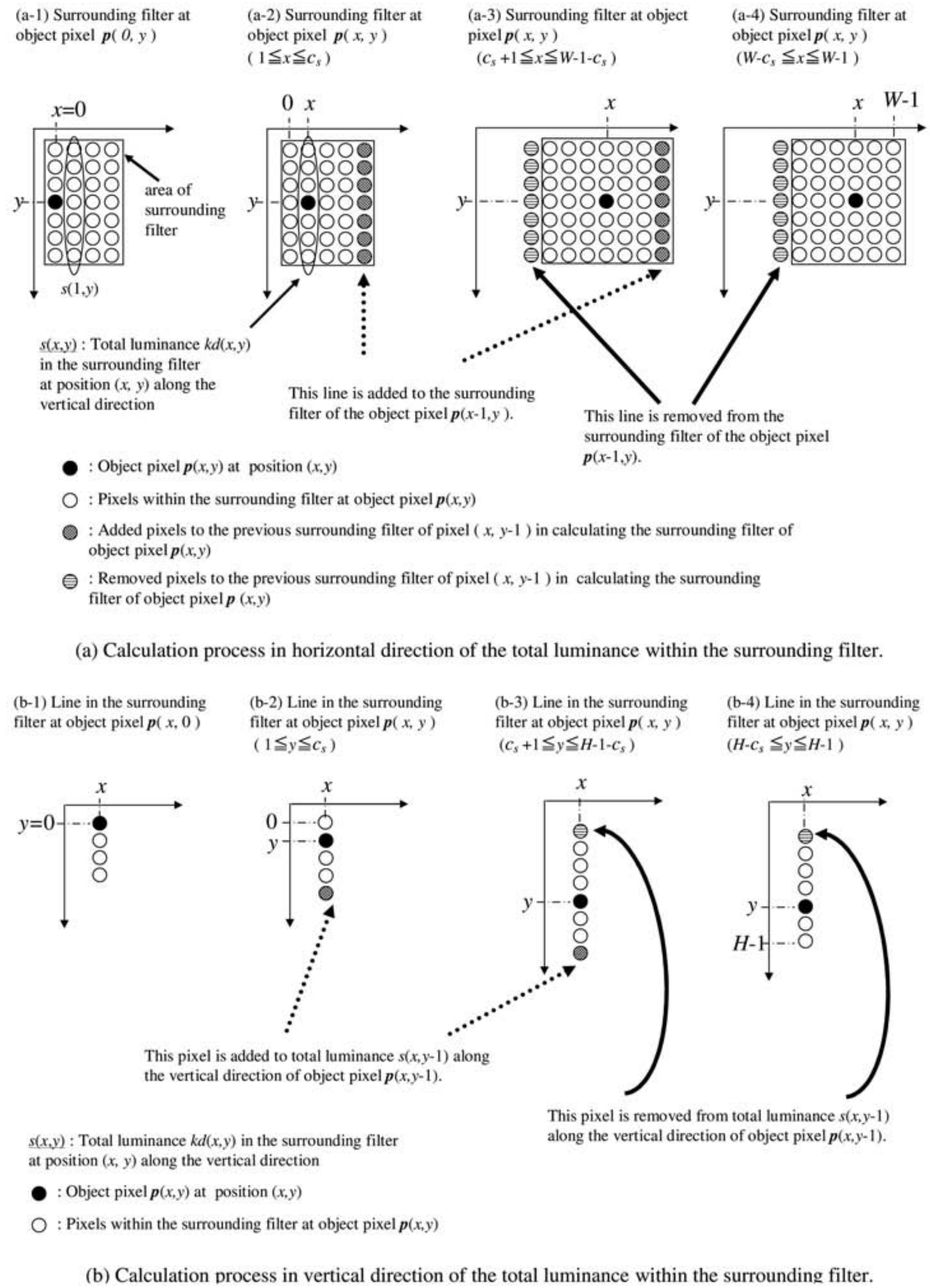

Figure 8. High-speed Calculation Process for Total Luminance within Surrounding Filter at Pixel $\boldsymbol{p}(x, y)$. (a) Calculation process in horizontal direction of the total luminance within the surrounding filter; (b) Calculation process in vertical direction of the total luminance within the surrounding filter.

The slope *Keisu* of a linearly controlled region is adjusted as shown in Fig. 7(b). *ThresCrCb* shows the threshold value of improved luminance, and *Keisu* shows the slope of the linear function between *MinR* and *MaxR* given by Eq. (13). *MaxK* shows the maximum value of *Keisu* and is a positive constant. As shown in Fig. 7(b) and Eq. (14), the *Keisu* is a constant value in case *outK* is smaller than *ThresCrCb*. In case *outK* is larger than *ThresCrCb*, *Keisu* linearly decreases, because the human eye is sensitive to a small amount of cyan color occurring in a highlight area. Consequently, in case *outK* is larger than *ThresCrCb*, the slope of *Keisu* linearly decreases according to Eq. (14) due to improved appearance in a highlight area.

Improvement in Processing Speed

The following three points are considered in order to achieve higher processing speed: (1) reduce the number of applied Gaussian functions, (2) simplify overall processing and (3) reduce the scale size.

(1) *Reduce the Number of Applied Gaussian Functions*

As shown above, the Retinex output of luminance is calculated instead of the Retinex output of each R, G and B component by Eq. (8), and the color difference signals are adjusted by the ratio of the improved luminance to the input luminance. In addition, $Ak(x, y, c_s)$ in Eq. (15) is defined by Eq. (16) instead of Eq. (9). That is, $Ak(x, y, c_s)$ shows the average luminance of the

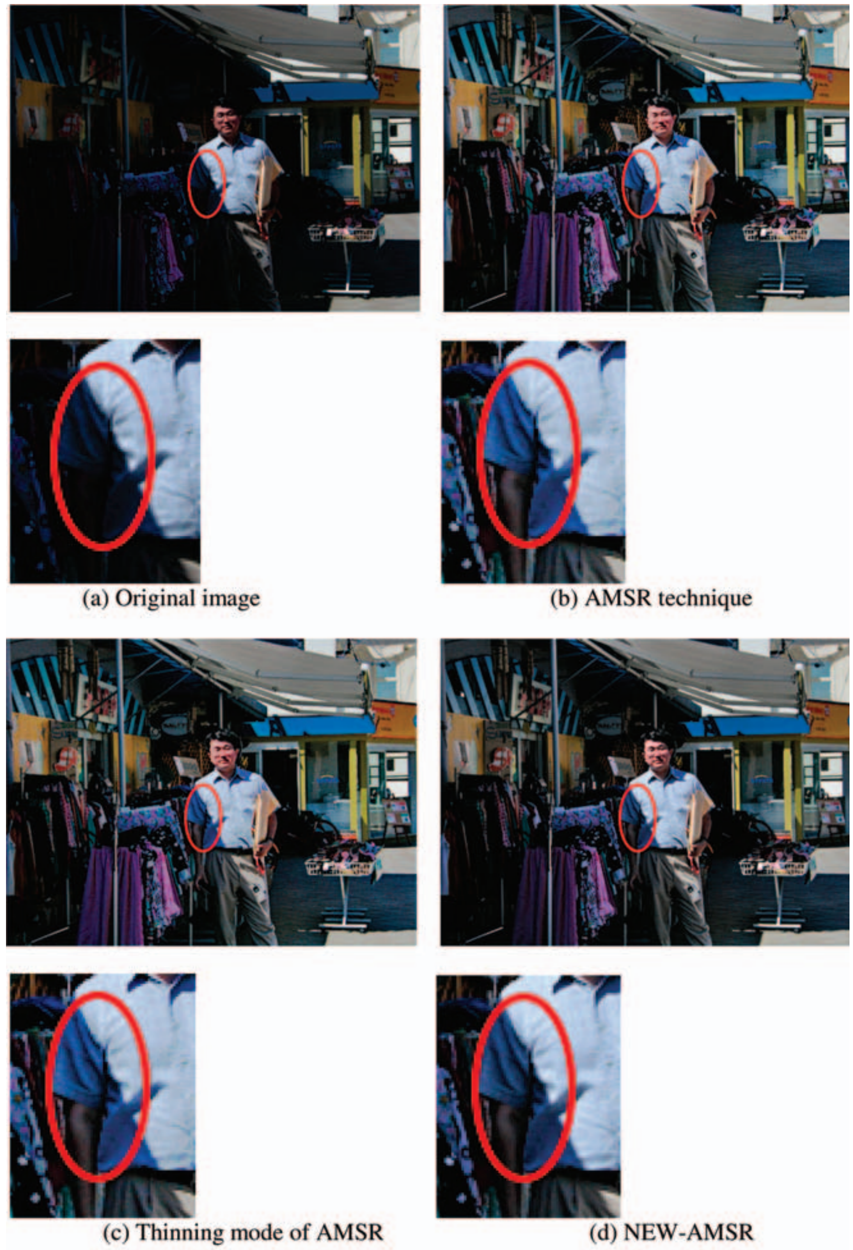

Figure 9. Image Quality Comparison of AMSR, Thinning Mode of AMSR and NEW-AMSR. (a) Original images; (b) AMSR technique; (c) Thinning mode of AMSR; and (d) NEW-AMSR.

surrounding pixels relative to the pixel under consideration. The surrounding field gs in Eq. (16) shows the surrounding field with the scale size c_s, and N_{gs} shows the number of the surrounding pixels in the surrounding field gs obtained by the process described below, reduces the scale size. The variable $kd(x, y)$ shows the luminance at position (x, y), which is the value between minimum luminance $THLow$ and maximum luminance $THHigh$ as shown in Eq. (17).

$$AR_i(x,y) = \sum_s w_s \, {k(x,y)}/{Ak(x,y,c_s)} \tag{15}$$

$$Ak(x,y,c_s) = \sum_{i \in gs} kd(x,y)/N_{gs} \tag{16}$$

$$kd(i,j) = \begin{cases} THLow & if\ k(i,j) \le THLow \\ THHigh & if\ k(i,j) \ge THHigh \\ k(i,j) & others \end{cases} \tag{17}$$

(2) *Simplify Overall Processing*

Additional processing of the edge emphasis component $Deki(x, y)$ in AMSR was simplified. Instead of additional processing of the edge emphasis component, the transform value Ct in process (3) of AMSR is controlled according to the luminance of the pixel under consideration. Eq. (18) shows the transform value function $Ct = CtFunc(k(x, y))$.

$$Ct = CtFunc(k(x,y)) = Ctc + dCt \cdot (k(x,y) - Kc) \tag{18}$$

TABLE I. Ratio of Thinning Out of Surrounding Pixels for Each Scale Size

	$c_0 = 126$	$c_1 = 30$	$c_2 = 6$
(a) Thinning mode of AMSR[19]	1/36	1/9	1
(b) NEW-AMSR	1/2	1/2	1/2

where Ctc, dCt and Kc denote the fundamental value of the transform value Ct, the changed value of transform value Ct and the fundamental luminance, respectively.

(3) *Reduce the Scale Size*

Improved processing speed was attempted by combining thinning out along the horizontal direction and serial processing to calculate total luminance within the surrounding filter. The ratio of thinning out in the horizontal direction for each scale size Cs is shown in Table I(b). Figure 8 provides an outline of the serial processing to calculate the total luminance within the surrounding filter. $\boldsymbol{P}(x, y)$ shows an object pixel at position (x, y) and $2c_s + 1$ shows the surrounding filter size to calculate surrounding luminance. W and H present the number of pixels along the horizontal direction in the input image and the number of pixels along the vertical direction in the input image, respectively.

[a] Firstly, total luminance $s(x, y)$ of $kd(x, y)$ at position (x, y) along the vertical direction in the surrounding filter is calculated up to $(0 \leq x \leq W - 1)$. Here, $kd(x, y)$ shows the luminance obtained by Eq. (17) at position (x, y) and the values are used when calculating the average luminance in the surrounding filter.

Then, the calculation process for the total luminance value $Ak(x, y)$ of the surrounding pixels to the pixel under consideration can be classified by four patterns according to the value of x $(0 \leq x \leq W - 1)$. $Ak(x, y)$ in each pattern can be calculated by the following formulas.

[a-1] At $x = 0$, the total luminance value $Ak(0, y)$ is calculated as the total value of $s(t,y)$ for z $(0 \leq t \leq c_s)$. Eq. (19) and Fig. 8 (a-1) show the case of $Ak(0,y)$.

$$Ak(0, y, c_s) = \sum_{t=0}^{C_s} s(t, 0) \tag{19}$$

[a-2] Figure 8 (a-2) shows an outline of the surrounding filter in the case that x is in the region $(1 \leq x \leq c_s)$. The area of the surrounding filter is obtained by adding the $(x + c_s)$ column to the area of the surrounding filter at $(x - 1, y)$. Therefore, total luminance $Ak(x, y)$ within $(1 \leq x \leq c_s)$ is calculated by adding the luminance sum $s(x + c_s, y)$ at position $(x + c_s, y)$ to $Ak(x - 1, y)$ at the previous column $(x - 1, y)$.

$$Ak(x, y, c_s) = Ak(x-1, y, c_s) + s(x + c_s, y) \tag{20}$$

[a-3] Figure 8 (a-3) shows an outline of the surrounding filter in the case that x is in the region $(c_s + 1 \leq x \leq W - 1 - c_s)$. The area of the surrounding filter is obtained by adding the $(x + c_s)$ column to the area of the surrounding filter at position $(x - 1, y)$ and subtracting the column $(x - (c_s + 1), y)$ from the area of the surrounding filter at position $(x - 1, y)$. Therefore, the total luminance $Ak(x, y)$ in the region $(c_s + 1 \leq x \leq W - 1 - c_s)$ is calculated by adding the luminance sum $s(x + c_s, y)$ at position $(x + c_s, y)$ along the y direction to $Ak(x - 1, y)$, and subtracting the luminance sum $s(x - (c_s + 1), y)$ at position $(x - (c_s + 1), y)$ to the total luminance $Ak(x - 1, y)$.

$$\begin{aligned} &Ak(x, y, c_s) = \\ &Ak(x-1, y, c_s) + s(x + c_s, y) - s(x - (c_s + 1), y) \end{aligned} \tag{21}$$

[a-4] Figure 8 (a-4) shows an outline of the surrounding filter in the case x is included in the region $(W - c_s \leq x \leq W - 1)$. A new area for the surrounding filter is presented as the area obtained by subtracting column $(x - (c_s + 1))$ from the area of the surrounding filter at position $(x - 1, y)$. Consequently, the total luminance $Ak(x, y)$ in the region $(W - c_s \leq x \leq W - 1)$ is calculated by subtracting the luminance sum $s(x - (c_s + 1), y)$ at position $(x - (c_s + 1), y)$ along the y direction from $Ak(x - 1, y)$ at the previous column $(x - 1, y)$.

$$Ak(x, y, c_s) = Ak(x-1, y, c_s) - s(x - (c_s + 1), y) \tag{22}$$

[b] On the other hand, total luminance $kd(x, y)$ in the surrounding filter at position (x, y) along the vertical direction $s(x, y)$ is classified into four cases. This is shown in Fig. 8(b) in the case of $x = 0$. Outlines of each case, $y = 0$, y in the region $(1 \leq y \leq c_s)$, y in the region $(c_s + 1 \leq y \leq H - 1 - c_s)$ and y in the region $(H - c_s \leq y \leq H - 1)$ are shown in Fig. 8 (b-1), (b-2), (b-3), and (b-4), respectively.

[b-1] Total luminance $kd(x, y)$ in the surrounding filter at position $(x, 0)$ along the vertical direction $s(x, 0)$ is calculated by Eq. (23) as the total value of $kd(x, u)$ for $k(x, u)$ in the region $(0 \leq u \leq c_s)$.

$$s(x, 0) = \sum_{u=0}^{C_s} kd(x, u), \quad s(x+1, 0) = s(x, 0) \tag{23}$$

[b-2] In the case of y being in the region $(1 \leq y \leq c_s)$, $s(x, 0)$ can be calculated as the value added to the conversion luminance value $kd(x, y + cs)$ at position $(x, y + c_s)$ to $s(x, y - 1)$ at position $(x, y - 1)$.

$$\begin{aligned} &s(x, y) = s(x, y-1) + kd(x, y + c_s), \\ &s(x+1, y) = s(x, y) \end{aligned} \tag{24}$$

[b-3] In the case of y being in the region $(c_s + 1 \leq y \leq H - 1 - c_s)$, $s(x, 0)$ can be obtained by adding the luminance value $kd(x, y + c_s)$ at position $(x, y + c_s)$ to $s(x, y - 1)$ at position $(x, y - 1)$, and subtracting the luminance value $kd(x, y - (c_s + 1))$ at $(x, y - (c_s + 1))$ as shown in Eq. (25).

$$\begin{aligned} s(x, y) = s(x, y-1) &+ kd(x, y + c_s) \\ &- kd(x, y - (c_s + 1)), s(x+1, y) = s(x, y) \end{aligned} \tag{25}$$

[b-4] In the case of y being in the region $(H - c_s \leq y \leq H - 1)$, the processing step is shown by Fig. 8 (b-4).

Then, $s(x, 0)$ is obtained by subtracting the luminance value $kd(x, y - (c_s + 1))$ at position $(x, y - (c_s + 1))$ to $s(x, y - 1)$ at position $(x, y - 1)$.

$$s(x,y) = s(x,y-1) - kd(x, y-(c_s+1)), \quad s(x+1,y) = s(x,y) \tag{26}$$

The sum of luminance $s(x, 0)$ at position $(x, 0)$ in the region $(0 \le x \le W-1)$ is first calculated. The total luminance value $Ak(0, 0)$ in the luminance of the surrounding filter at position (0, 0) is then calculated using $s(x, 0)$. Next, total luminance $Ak(x, y)$ at the remaining position (x, y) in the surrounding filter $(1 \le x \le W-1,\ 0 \le y \le H-1)$ can be obtained by several addition and subtraction calculations.

Therefore, the number of calculations needed to determine total luminance in the surrounding filter for each pixel in the input image can be greatly reduced by the serial processing indicated above.

Experimental Results

Efforts to improve color balance and processing speed were made as described below.

A comparison of experimental results for AMSR, the thinning mode of AMSR presented in a Ref. [19], and NEW-AMSR as described in above was carried out. The original image was taken with a DSC, and the experimental conditions were the same as described above. The rate of thinning out presented in Table I is defined as the ratio of the number of pixels used to calculate average luminance $Ak(x, y, c_s)$ to the number of pixels within scale size c_s. When calculating $Ak(x, y, c_s)$, the number of object pixels decreases according to the rate of thinning out and faster processing can be achieved.

Table I(a) shows the rate of thinning out applied in the Ref. [19] and Table I(b) shows the rate of thinning out to achieve the high speed processing as described above.

For the processing directed towards improved color appearance, $ThresCrCb$ = 223, $CMax$ = 2.0, $CMin$ = 1.0 and $MaxK$ = 0.5 were used. For the processing directed toward improved processing speed by simplification of overall processing, dCt = 0.2, Kc = 128 and Ctc = 120 were used.

The experimental results are shown in Fig. 9. The cropped images given in (a), (b), (c), and (d) show the original image, the output image from AMSR, the thinning mode of AMSR, and NEW-AMSR, respectively. As shown in Fig. 9, (b), (c) and (d) have been improved visually so that the detail in the dark area is clearer than the original image in (a). Comparing (b) and (c), in spite of the calculation of average luminance $Ak(x, y, c_s)$ by applying a high rate of thinning out of the surrounding pixels, there is visually no significant difference in image quality.

However, the appearance of a difference in cyan color caused by a slight color unbalance in the R, G and B channels can be observed in the area within the red line in the dark area of (b) and (c). On the contrary, such a color unbalance cannot be observed in (d). Such a color unbalance was not observed in any output image processed by AMSR or the thinning mode of AMSR. Regarding the improvement of color appearance, it was confirmed that NEW-AMSR was more effective than AMSR and the thinning mode of AMSR based on our examination of a large number of images.

In accordance with the above results, it was concluded that NEW-AMSR can enhance visibility in dark areas while maintaining both color balance and saturation, in comparison with conventional histogram equalization, MSR as proposed by Jobson, and AMSR proposed in the Ref. [19].

Next, we compared the processing time of AMSR, the thinning mode of AMSR[19] and the NEW-AMSR. Table II shows the observed results. Here, the processing time was measured by computer simulation using a PC-AT personal computer with a Pentium 4 (2.0GHz) CPU, 768 MB of RAM and Windows XP.

TABLE II. Comparison of Processing Time for Each Technique

	Processing time (sec)
(b) AMSR technique	327.51
(c) Thinning mode of AMSR[19]	7.00
(d) NEW-AMSR	0.20

As shown in Table II, the processing time for the thinning mode of AMSR is about fifty times faster than that of AMSR, while the processing time for NEW-AMSR is about thirty times faster than that of the thinning mode of AMSR. It is evident that the number of processing steps for NEW-AMSR is smaller than that for the thinning mode of AMSR. Moreover, this result shows that the processing time of NEW-AMSR represents a significant improvement over the much slower performance of AMSR and conventional MSR.

From the above results, the NEW-AMSR proposed in this paper can be achieved by combining a low ratio of thinning out in the horizontal direction with serial processing in the calculation of total luminance in the surrounding filter.

Conclusions and Future Work

The human vision system almost effortlessly performs the tasks of dynamic range compression and color constancy. This is a very challenging issue for electronic imaging systems because dynamic range is limited by the CCD device characteristics of a DSC. In order to improve dynamic range, Land, McCann, and Jobson studied various techniques based on the Retinex theory. A representative technique is Multi-scale Retinex (MSR). This technique, however, raises issues concerning color correction of images printed with a different RGB density distribution. In this paper we have proposed Adaptive Multi-scale Retinex (AMSR) to address the issues associated with MSR. The AMSR technique is characterized by linear computation and synthesis of both the original image and the image processed by MSR. With the simulation of printed DSC images, we have shown that AMSR enhances visibility in dark areas while maintaining both color balance and saturation. This compares very favorably with both conventional histogram equalization and the MSR technique proposed by Jobson.[13–16] AMSR suppresses both the appearance of noise in dark areas and the decrease of luminance in the highlight areas.

Moreover, we attempted to improve the level of chromatic unbalance in dark areas, and to reduce AMSR processing time. In order to improve the level of chromatic unbalance, improvement of luminance in the input image was carried out using AMSR and two color differences were controlled by improved luminance without enhancement of each R, G and B channel. To reduce processing time, we proposed NEW-AMSR that combines a low ratio of thinning out in the horizontal direction with only serial processing in calculation of the average within a surrounding filter. Simulation results showed that a color unbalance in dark areas could be suppressed more efficiently with NEW-AMSR. We also showed that the processing speed of NEW-AMSR was about fifty times faster than the thinning mode of AMSR and about one thousand times faster than AMSR and MSR.

Regarding future work, we will further investigate AMSR high speed processing and the reduction of memory capacity requirement. As another issue, it is said that printed DSC color images are not generally consistent with the visual color perceived by human eyes. This phenomenon is due to the observation of a scene under different illumination conditions (a color constancy problem). A practical next step is to address this color constancy issue for a variety of application purposes, and we will be extending NEW-AMSR to include color constancy under various illuminant conditions.

Acknowledgment. The authors wish to thank Dr. Hiroaki Kotera of department of information and faculty of image sciences engineering, Chiba University for his valuable advices on this study.

References

1. K. N. Plataniotis, A. Lacroix and A. Venetsanoupoulos, *Color Image Processing and Applications*, (Springer Verlag, Wien, 2000).
2. R. C. Gonzalez and P. Wintz, *Digital Image Processing-Reading*, 2nd ed. (Addison-Wesley, Reading, MA, 1987).
3. R. A. Hummel, "Image Enhancement by Histogram Transformation," *Computer Graphics and Image Processing*, **6**, 184–195 (1977).
4. S. M. Pizer, "Adaptive Histogram Equalization and Its Variations," *Computer Vision, Graphics, and Image Processing*, **39**, 355–368 (1987).
5. D. Marr, *Vision : A Computational Investigation into the Human Representation and Processing of Visual Information*, (W. H. Freeman, New York, 1982).
6. E. H. Land and J. J. McCann, "Lightness and Retinex Theory," *J. Opt. Soc. Amer*, **61**, 1–11 (1971).
7. E. H. Land, "An Alternative Technique for the Computation of the Designator in the Retinex Theory of Color Vision," *Proc. Nat'l. Acad. Sci.*, **83**, 3078–3080 (1986).
8. A. C. Hurlbert and T. Poggio, "Synthesizing a Color Algorithm from Examples," *Science*, 239, 482–485 (1988).
9. A. Moore, J. Allman and R. M. Goodman, "A Real-time Neural System for Color Constancy," *IEEE Trans. Neural Networks*, **2**, 237–247 (1991).
10. J. J. McCann, "Lessons Learned from Mondrians Applied to Real Images and Color Gamuts," *Proc. IS & T / SID 7th Color Imaging Conference*, (IS&T, Springfield, VA, 1999) pp. 1–8.
11. B. V. Funt, F. Ciurea and J. J. McCann, "Retinex in Matlab," *Proc. IS & T / SID Eighth Color Imaging Conference*, (IS&T, Springfield, VA, 2000) pp. 112–121.
12. Z. Rahman, "Properties of a Center/Surround Retinex, and Part One: Signal Processing Design," *NASA Contractor Report,* 198194, (1995).
13. D. J. Jobson and G. A. Woodell, "Properties of a Center /Surround Retinex and Part Two: Surround Design," *NASA Technical Memorandum* 110188 (1995).
14. D. J. Jobson, Z. Rahman and G. A. Woodell, "Retinex Image Processing: Improved Fidelity to Direct Visual Observation," *Proc. IS&T/SID Fourth Color Imaging Conference: Color Science, Systems and Applications*, (IS&T, Springfield, VA, 1996) pp. 124–126.
15. D. J. Jobson, Z. Rahman and G. A. Woodell, "Properties and Performance of a Center/Surround Retinex," *IEEE Trans. Image Processing*, **6**, 451–462 (1997).
16. D. J. Jobson, Z. Rahman and G. A. Woodell, "A Multiscale Retinex for Bridging the Gap Between Color Images and the Human Observation of Scenes," *IEEE Trans. Image Processing*, **6**, 965–977 (1997).
17. Z. Rahman, D. Jobson and G. A. Woodel, "A Multiscale Retinex for Color Rendition and Dynamic Range Compression," *Proc. SPIE* **2847,** pp. 183–191 (1996).
18. M. Fujita, M. Kobayashi, Y. Hashimoto and H. Kotera, "Appearance Improvement of Color Image by Retinex Model," *Proc. International Congress of Imaging Science 2002*, (SPSTJ, Tokyo, Japan, 2002) pp. 590–591.
19. T. Watanabe, Y. Kuwahara, A. Kojima and T. Kurosawa, "Improvement of Color Quality with Modified Linear Multi-scale Retinex," *Proc. SPIE* **5008**, 59–69 (2003).